IEEE Photonics Journal
An IEEE Photonics Society Publication

Inspection of Intraocular Lens With Dual-Side View Optical Coherence Tomography

Volume 13, Number 3, June 2021

Qian Wu
Xiwen Wang
Linbo Liu
Jianhua Mo

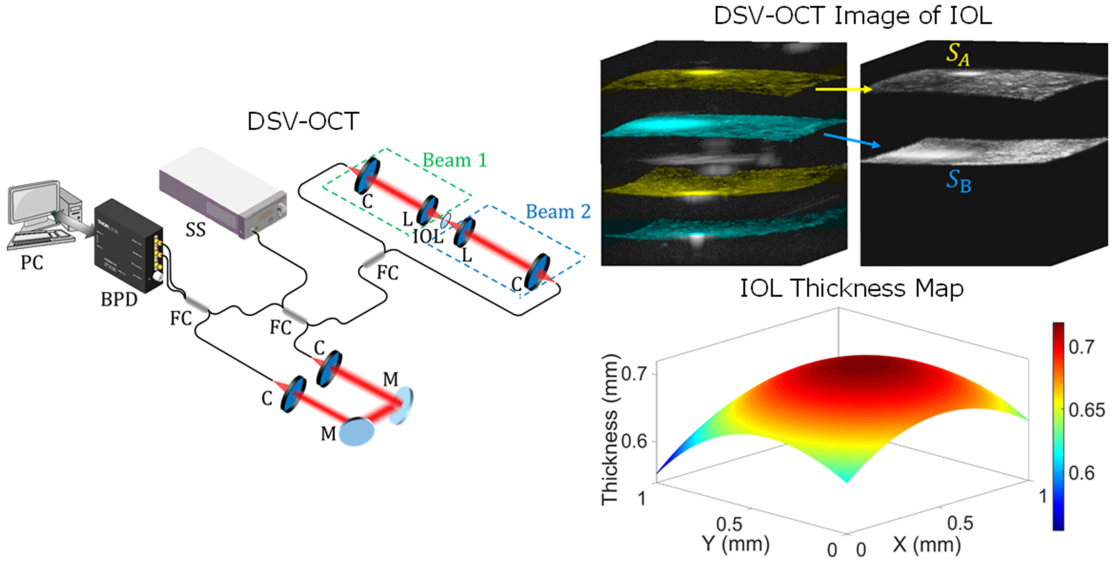

DOI: 10.1109/JPHOT.2021.3080498

Inspection of Intraocular Lens With Dual-Side View Optical Coherence Tomography

Qian Wu,[1] **Xiwen Wang**,[1] **Linbo Liu**,[2] **and Jianhua Mo**[1]

[1]School of Electronics and Information Engineering, Soochow University, Suzhou 215006, China
[2]School of Electrical & Electronic Engineering, Nanyang Technological University, Singapore 639798, Singapore

DOI:10.1109/JPHOT.2021.3080498

Manuscript received April 13, 2021; revised May 11, 2021; accepted May 12, 2021. Date of publication May 14, 2021; date of current version June 10, 2021. This work was supported in part by the National Natural Science Foundation of China under Grant 81401451, in part by the Natural Science Foundation of the Jiangsu Province under Grant BK20140365, in part by the Postgraduate Research & Practice Innovation Program of Jiangsu Province under Grant 5832001320, in part by the Singapore Ministry of Health's National Medical Research Council under its Open Fund Individual Research under Grant MOH-OFIRG19may-0009, and in part by the Ministry of Education Singapore under its Academic Research Fund under Grants 2018-T1-001-144 and T2EP30120-0001. Corresponding author: Jianhua Mo (e-mail: joshuamo@gmail.com).

Abstract: Intraocular lens (IOL) is widely used for cataract treatment. Its optical properties are crucial to obtain a good treatment efficacy and thus need to be evaluated and controlled. In this study, we propose a novel method based on optical coherence tomography (OCT) for noncontact and accurate *in vitro* measurement of thickness, refractive index and dioptric power of IOL implants. The OCT setup is specially designed to create two sampling optics, called dual-side view OCT (DSV-OCT), which allows for imaging IOL from the two opposite sides simultaneously in single OCT volume scanning. This can produce a three-dimensional surface contour without suffering image distortions due to the refraction of the curved surface. Then, the thickness and surface curvature can be easily computed from the surface contours. In addition, DSV-OCT is able to measure the refractive index. Three IOLs with different dioptric powers (5D, 20D and 28D) were chosen to evaluate this method. The results show that this method is capable to provide a comprehensive and accurate evaluation of IOLs from the aspects of thickness, refractive index and dioptric power, and hence can be potentially used as a quality assurance tool by IOL manufacturers.

Index Terms: Optical coherence tomography, dual-side view, intraocular lens, inspection, *in vitro* measurement.

1. Introduction

Cataract is one of the common eye diseases in the aging population. More than 65.2 million people worldwide have cataracts according to the first world report on vision issued by the World Health Organization in 2019 [1]. Given that cataracts get worse over time, people left untreated will experience increasingly severe vision impairment which can lead to blindness. The common treatment for cataract is the replacement of the natural lens by an intraocular lens (IOL). IOL implantation in refractive cataract surgery has become one of the most commonly performed surgical operations in medicine since the first implantation of IOLs [2]. Most of the cataract post-surgical

device-associated complications are directly related to some fundamental IOL optical properties such as dioptric power, imaging quality, refractive index (RI), thickness, and geometrical shape [3]. Some new designs have led to additional complications resulting in explantation to realign or exchange the lens [4]. As a result, effective and accurate measurement on IOL optical properties before IOL implantation is highly desired in order to reduce IOL complications.

Dioptric power, equivalent to the reciprocal of effective focal length (EFL), is the leading key parameter of IOL, which determines the treatment efficacy of cataract with IOL implantation. Conventional EFL measurement techniques are developed based on paraxial optics theory, such as nodal slide method [5]. Many of these techniques, however, usually require rigorous alignment, which places a big impact on the measurement accuracy. There also exist other methods based on diffraction theory, such as Moiré deflectometry and Talbot interferometry [6], [7]. The measurement accuracy is mainly limited by fringe counting for Moiré deflectometry, and distance measurement between Moiré images for Talbot interferometry. However, these methods are not well suited for lens with small aperture and short focal length, for example, IOLs. Thus, new measurement methods have being developed. For instance, confocal optical fiber laser microscopy is proposed as an improved alternative to those conventional techniques for its advantages of good accuracy, objective and efficient measurement [8]. However, it still requires certain preliminary system alignment as well as additional lens thickness measurement. The same group reported another confocal fiber optic laser method, which however requires more separate measurements on various parameters for EFL calculation [9].

Besides, refractive index and central thickness are another two important parameters as part of release specifications for all IOLs and are of critical importance to the safety and effectiveness of IOLs. Moreover, these two parameters determine the dioptric power. Usually, thickness can be measured with micrometer or Vernier caliper. These methods require contact with the sample and consequently it is inevitable to destroy the surface quality of IOLs. Moreover, it is hard to position the measurement tool accurately at the center of IOLs for central thickness measurement. As for refractive index, refractometer is one of the common measurement tools. But the curved surface of IOLs may cause errors to the measurement.

In this study, we propose to employ dual-side view optical coherence tomography (DSV-OCT) as a single-shot solution for thickness, refractive index and dioptric power measurements of IOLs. OCT is a non-destructive and non-contact three-dimensional optical imaging tool, which has achieved a great success in various medical diagnosis fields, such as ophthalmology [10], [11], dermatology [12], cardiology [13] and gastroenterology [14]. Meanwhile, OCT has also found various uses in industrial non-destructive evaluation (NDE), such as inspection of pearl [15], art objects [16], industrial ceramics [17], pharmaceutical tablet coating [18], conformal coating [19] and so on. In particular for IOL, OCT has been often used to predict the postoperative position of IOL *in vivo* [20], [21].

In contrast, use of OCT in quality assessment of IOL is very limited. Although a few studies have attempted to measure the thickness and refractive index of biological tissues [22]–[24], the refractive errors caused by the curvature of the sample surface were ignored, which is not valid for *in vitro* IOL measurement. To tackle the limitation, common-path Fourier domain optical coherence tomography has been employed to measure the two surfaces of IOL separately by only measuring the surface reflected light [25]. However, in the experiment, IOL needs to be flipped along the optic axis to switch the measurement between the two surfaces, which may result in additional errors. The flipping procedure can be eliminated by the dual-side imaging capability of DSV-OCT [26]. Specifically, DSV-OCT is armed with two sampling light beams, which allow for imaging the two surfaces simultaneously in reflection mode. This can yield the surface profiles in physical thickness of IOL which is free of optical distortions caused by the light refraction at the curved surfaces [27]. The refractive index of IOL can be simply calculated as the ratio between the optical thickness and physical thickness measured by DSV-OCT. In this work, we demonstrated the capability of DSV-OCT to measure IOL's surface profile, thickness distribution, refractive index and dioptric power by single three-dimensional volume imaging, which can potentially push OCT forward as an effective quality-assurance tool in IOL industry.

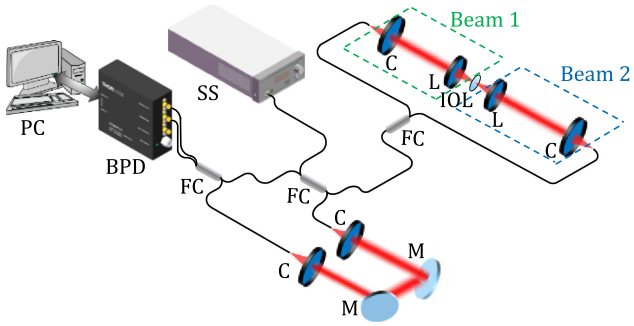

Fig. 1. Schematic of dual-side view swept source OCT system. SS: swept source; FC: fiber coupler; C: collimator; M: mirror; BPD: balanced.

2. Methods

2.1 Experimental Setup

A specially developed fiber-optic OCT, called dual-side view OCT, was employed for imaging intraocular lens. The system has been described in detail elsewhere [26]. Fig. 1 shows the schematic of the system, which was built based on Michelson interferometer. Specifically, the light from the swept source is split into the sample and reference arms by a 50:50 fiber coupler. The one-way path reference arm was constructed with a pair of identical collimators (F220APC-1064, Thorlabs Inc., Newtown, NJ, USA). The sample arm is specially designed to create two sets of sampling optics with a 1×2 fiber coupler. Each sampling optics consists of a collimator (F220APC-1064, Thorlabs Inc., Newtown, NJ, USA) and a focusing lens (AC254-050-B-ML, Thorlabs Inc., Newtown, NJ, USA). The two sampling optics share the same focal plane and are positioned in left-right symmetry with respect to the sample. This allows for imaging the left-side and right-side surfaces of a sample simultaneously which is positioned at the focal plane. The light coming back from both sample and reference arms interferes at another 50:50 fiber coupler, and the interference signal is detected by a balanced photo-detector (PDB471C, 400MHz, Thorlabs, Newtown, NJ, USA) and further digitized with a 12 bit analog-to-digital converter (ATS9351, Alazartech, Pointe-Claire, QC, Canada). To provide B-scan and C-scan imaging, sample scanning is implemented by mounting the IOL on a two-dimensional translational stage, which is driven by a pair of DC servo electric actuators (Z812B, 12 mm travel, Thorlabs Inc., Newtown, NJ, USA). The actuators are driven by a custom-developed software on LabVIEW platform. For imaging IOL, our DSV-OCT collects contour information from both sides of the IOL in back reflection mode. This means that the light utilized for imaging does not undergo any interface refraction and therefore the measurement does not surfer from the image distortion due to the IOL's surface refraction [27].

2.2 Determination of IOL Key Parameters

2.2.1 Refractive Index: Note that the thickness measured by conventional OCT imaging is not physical thickness but optical thickness, which results from scaling physical thickness with refractive index. Thus, in order to measure the refractive index by OCT, additional physical thickness is required. Our DSV-OCT can measure not only optical thickness but also physical thickness, and therefore provide an ideal and effective way for refractive index measurement. In addition, it should be pointed out that the refractive index measured by the method above is actually the group index. The difference is negligible and therefore it is fair to approximate the refractive index of IOL with the group index measured with OCT [24].

Specifically for IOL's refractive index measurement, it needs to be pointed out that OCT image of IOL may be distorted due to the curved surface of IOL. As illustrated in Fig. 2(a), assuming that IOL is positioned vertically and the light (Beam 1 in Fig. 1) enters IOL horizontally from IOL's left side, the light can continue the horizontal path only when it hits the center of IOL (point C in Fig. 2(a)).

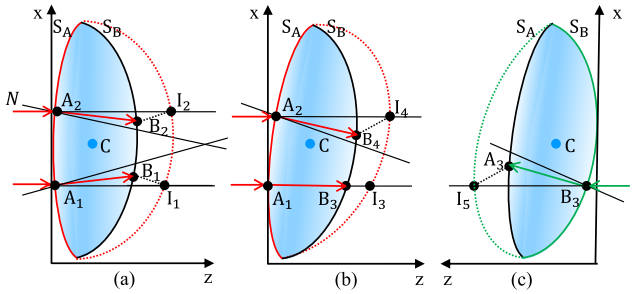

Fig. 2. OCT imaging cartoon of IOL: (a) IOL positioned vertically, (b)–(c) IOL positioned obliquely. Red and green arrows delineate the light paths of Beam 1 and Beam 2, respectively. Surfaces S_A and S_B denote the left and right surfaces of the IOL, respectively. OCT image of IOL by beam 1 is delineated with red solid and dotted curves while image by beam 2 is in green.

Otherwise, the light deviates from the original path due to the refraction induced by the curved surface. For example, in Fig. 2(a), the light gets into IOL from point A_1 on the left surface and is reflected backwards from point B_1 on the right surface. In OCT cross-sectional image, the light path of A_1-to-B_1 will be present as the path A_1-to-I_1, considered as the depth profile at point A_1. Eventually, the right surface will be distorted as depicted by the green dashed curve even though the vertical symmetry is retained as indicated by light paths A_1-B_1 (corresponding A-scan: A_1-I_1) and A_2-B_2 (corresponding A-scan: A_2-I_2). In addition, in practice, it is inevitable that the IOL may be slightly tilted. Fig. 2(b) shows the IOL tilted in X-Z plane as an example. This tilt destroys the vertical symmetry mentioned above. Specifically, the light at point A_2 suffers a larger refraction compared to the situation in Fig. 2(a) while smaller refraction at point A_1. This causes the image of surface S_B by Beam 1 to be stretched towards upper-right corner (depth scanning along A_2-B_4 shown as A-scan A_2-I_4 at A_2 in OCT image). To ease the description of the following refractive index calculation, a special situation is held by assuming Beam 1 to be incident normally at point A_1. Thus, the light at this point does not undergo any refraction, allowing for referring to the optical thickness of A_1-B_3 by A_1-I_3 in OCT image. The optical thickness above can be calculated as below:

$$OT_{A_1B_3} = z_{1I_3} - z_{1A_1} \tag{1}$$

where z_{1A_1} and z_{1I_3}represents depth positions of point A_1 and B_3 in OCT image by Beam 1, respectively. Note that in DSV-OCT, there is a second beam (Beam 2 in Fig. 1) to image IOL from its right side as shown in Fig. 2(c). According to thickness measurement theory by DSV-OCT, the physical thickness of A1-B3 can be determined using the following formula [26]:

$$PT_{A_1B_3} = 2z_{rp} - \left(z_{2B_3} + z_{1A_1}\right) \tag{2}$$

where z_{rp} represents the reference plane position in OCT image defined in [26], z_{2B_3}represents the depth position of point B_3 in OCT image by Beam 2. The optical thickness is divided by the physical thickness to obtain the refractive index:

$$\begin{aligned} n_{IOL} &= OT_{A_1B_3} / PT_{A_1B_3} \\ &= \left(z_{1I_3} - z_{1A_1}\right) / \left[2z_{rp} - \left(z_{2B_3} + z_{1A_1}\right)\right] \end{aligned} \tag{3}$$

In real experiment, the position where the light enters IOL normally is determined in three-dimensional space by searching for IOL's surface peak in OCT image, and then the calculation discussed above is performed to obtain IOL's refractive index.

2.2.2 Thickness: Thickness is one of the key parameters of IOL. In theory, our DSV-OCT can measure the physical thickness directly. Fig. 3(a) shows a cartoon mimicking the typical DSV-OCT cross-sectional image of IOL. The OCT images of surfaces S_A and S_B defined in Fig. 2 by Beam 1 and Beam 2 are colored with red and green, respectively. The axial gap between the two surfaces can be easily calculated according to the thickness measurement mechanism of

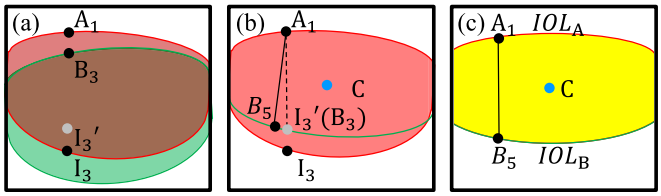

Fig. 3. IOL tilt effect correction process: (a) original B-scan image, (b) actual image, (c) tilt-corrected image. The areas marked in red is the B-scan of the IOL generated by Beam 1, while green is the B-scan of the IOL generated by Beam 2 in Fig. 3(a).

DSV-OCT [26]. Then, surface S_B can be flipped axially and separated from surface S_A with the physical thickness obtained above as depicted in Fig. 3(b). However, the IOL tilt in experiment leads to an error to physical thickness measured by DSV-OCT. For example, the real thickness at point A_1 should be the path length from point A_1 to B_5; apparently, due to the tilt effect discussed previously, the thickness is determined incorrectly with the path from A_1 to B_3. Consequently, the IOL tilt needs to be corrected prior to thickness measurement. The tilt correction is realized via two steps: (1) determine the position of the gravity center of the closed area between the upper and lower surfaces. The gravity center coordinate G(x,y) of the closed area is calculated as following:

$$\begin{cases} x = \left(\sum_{i=1}^{n} x_i\right)/n \\ y = \left(\sum_{i=1}^{n} y_i\right)/n \end{cases} \tag{4}$$

where x_i is the x-coordinate of the i-th pixel position, y_i is the y-coordinate of the i-th pixel position, n represents the total number of the pixels. (2) image is rotated around the gravity center to reposition the IOL image horizontally. The rotation angle is determined when the horizontal tangent points of the upper and lower surfaces are in the same lateral position. The depth positions of surfaces S_A and S_B after correcting the tilt are denoted as IOL_A and IOL_B, respectively. The physical thickness PT can be calculated with the axial gap between the two surface contours as below:

$$PT = (IOL_B - IOL_A) \times px \tag{5}$$

where px represent the pixel size in axial dimension.

In real measurement, the tilt correction is implemented in both fast-scan dimension and slow-scan dimension. Afterwards, the IOL surfaces were segmented by performing a peak detection on each A-scan; subsequently, a second order polynomial surface profile fitting was performed using the toolbox in MATLAB R2017b. The points with residual error over 4 pixels were excluded from the fitting data to improve the accuracy of fitting. With the fitted left and right surfaces, a two-dimensional thickness map can be yielded. In addition, it is reasonable to determine the central thickness of IOL by searching for the maximal thickness on the thickness map regardless if IOL is plano-convex or double-convex.

2.2.3 Dioptric Power: The dioptric power D_{IOL} can be computed based on the following formula [28]:

$$D_{IOL} = D_l + D_r - (d_c/n_{IOL}) \times D_l \times D_r \tag{6}$$

where d_c and n_{IOL} are the central thickness and refractive index of the IOL. D_l and D_r can be calculated as the equations below:

$$D_l = (n_{IOL} - n_{air})/r_l \tag{7}$$

$$D_r = (n_{air} - n_{IOL})/r_r \tag{8}$$

where r_l and r_r are the radii of the left and right surfaces of the IOL, respectively, and n_{air} is the refractive index of the air (1.0).

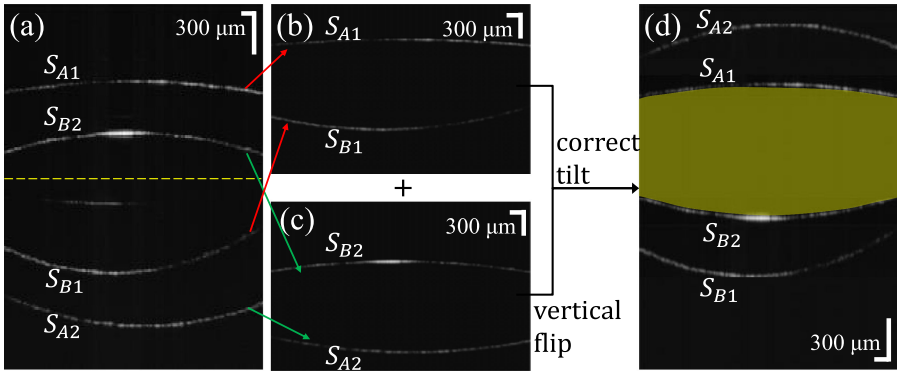

Fig. 4. (a) DSV-OCT image of IOL, (b) IOL image by Beam 1 extracted from (a), (c) IOL image by Beam 2 extracted from (a), (d) tilt-corrected image of IOL. Image lateral size: 3.2 mm.

IOL's refractive index (n_{IOL}) and central thickness (d_c) can be obtained as discussed in Section 2.2.1 and Section 2.2.2, respectively. As for IOL's surface radius, it can be obtained by surface fitting after obtaining the entire boundary of the intraocular lens.

3. Results

In this study, three different types of IOLs with dioptric powers of 5D, 20D and 28D (PC55125, EYEGOOD, China) were evaluated as examples of commonly used low-, middle-, and high-diopter IOLs, respectively. Fig. 4(a) depicts an example of IOL DSV-OCT image (20D). Four curved surfaces are found in the image, which are referred to as the IOL surfaces imaged by the two light beams in DSV-OCT imaging. Conventional OCT cross-sectional images of IOL by Beam 1 and Beam 2 are separated and shown in Figs. 4(b) and 4(c), respectively. Note that the two beams illuminate the IOL from the opposite sides separately, and therefore, the images of IOL by the two beams appear to be mirrored to each other. Surfaces denoted with S_{A1} and S_{A2} are referred to as surface S_A imaged by Beam 1 and Beam 2, respectively (surfaces denoted with S_{B1} and S_{B2} correspond to surface S_B). Besides, there is also an additional bright horizontal line, which can be attributed to the one-way pass of the light through the IOL between the two sampling optics.

It is clearly seen that surface S_{B1} was elongated towards bottom left and similar distortion happens on surface S_{A2} towards bottom right. This distortion can be explained by the fact that the light beam was refracted when hitting the incident curved surface as well as the tilt of IOL during imaging. This has been discussed in depth in Section 2.2.1. In comparison, surface S_{A1} and surface S_{B2} did not suffer sort of distortion because these two surfaces were imaged based on exclusive surface reflection. This guarantees the symmetry of these two surfaces even though they were tilted a little bit. Consequently, by using DSV-OCT imaging, the distortion effect can be eliminated simply by using the two undistorted surfaces of IOL. In detail, surface S_{B2} is flipped vertically and subsequently fused with surface S_{A1} in the same B-scan as seen in Fig. 4(d) to create a distortion-free IOL's surface profile. The vertical separation of the two surfaces can be determined according to the working principle of DSV-OCT with the reference plane delineated with yellow dashed line in Fig. 4(a). Then, the resultant image matches the actual shape of IOL. Again, it is clearly seen that surface S_{A2} exhibits a larger curvature than surface S_{A1}. This is because Beam 2 is refracted by surface S_B before reaching surface S_A when imaging surface S_A. Similar finding was observed on surface S_{B1} and surface S_{B2}. Besides, as mentioned early, the image is slightly tilted, which is hard to avoid when IOL is held vertically for imaging. This will cause an error in physical thickness measurement as discussed in Section 2.2.2. Consequently, this tilt is corrected by rotating IOL image around its gravity center before extracting the physical thickness from this image. The shape filled with yellow color matches the real shape of IOL exactly.

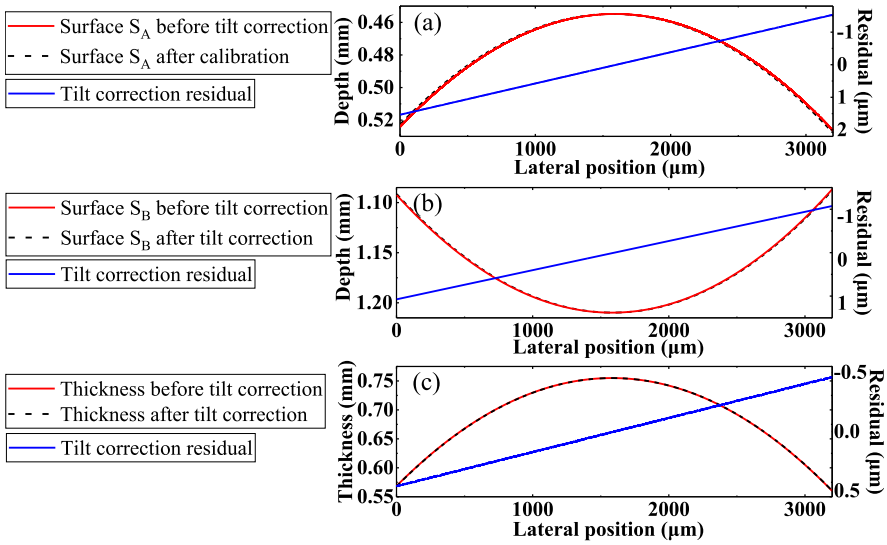

Fig. 5. Tilt effect evaluation on surface profile: (a) surface S_A, (b) surface S_B, and (c) on thickness measurement. Surfaces S_A and S_B denote the left and right surfaces of the IOL, respectively.

To measure the physical thickness of IOL, IOL's surfaces in OCT image are segmented with peak detection method which is repeated on each image column. Subsequently, the segmented surfaces are fitted with a second order polynomial, which is eventually utilized for thickness calculation. Figs 5(a)–(b) describe the lateral profiles of surfaces S_A and S_B before and after tilt correction. It seems that the tilt is subtle, as illustrated by the difference between the original surface and tilt-corrected surface (blue curves in Figs. 5(a)–(b)). It is seen that the deviation of surface depth position increases nearly linearly from the center towards the edge. The increase slope is about 0.001 for surface S_A, which is twice larger than that (0.0005) for surface S_B. This implies that the tilt places a bigger impact on the surface with larger curvature. When calculating the thickness with the two surface profiles above, the tilt effects on both surfaces cancelled each other significantly. This is illustrated in Fig. 5(c) that the tilt correction residual is below 0.5 um for thickness profile while the residual is up to be more than 1 um for surface profile (Figs. 5(a)–(b)). As the effect of tilt on thickness measurement is at sub-micrometer range, it can be neglected in this situation. In our work, tilt effect correction is conducted for all the measurements to secure the measurement accuracy.

To measure IOL's optical properties, the IOL was scanned around its center with a 1x1 mm area to produce a three-dimensional image. Fig. 6(a) describes the 3D volume image of 20D IOL (left panel). The images produced by Beam 1 and Beam 2 are delineated with yellow and cyan colors, respectively. Firstly, we calculate the optical thickness and physical thickness by the A-scan at the horizontal tangent point of left surface, which are 1.068 mm and 0.717 mm, respectively, according to the method described in Section 2.2.1. Then, the refractive index was calculated to be 1.490 according to Eq. (3). The result matches well to the known value 1.492 provided by the manufacturer. Secondly, surface S_A by Beam 1 and surface S_B by Beam 2 are extracted and undergo the tilt-correction in both fast-scan and slow-scan dimensions to produce a tilt-free three-dimensional image of IOL (right panel of Fig. 6(a)). The overall contour of the surfaces can be clearly seen from the three-dimensional image. Thirdly, the surfaces are segmented as denoted with blue scatterers in top panel of Fig. 6(b). Subsequently, the segmented surfaces are fitted with a second order polynomial surface function. The points in the segmented surfaces that deviate from the fitting surface by more than 4 pixels are excluded from the fitting process to improve the fitting accuracy as delineated with red cross in top panel of Fig. 6(b). The corresponding fitting residual is presented in bottom panel of Fig. 6(b). The fitted surface S_A and surface S_B are shown

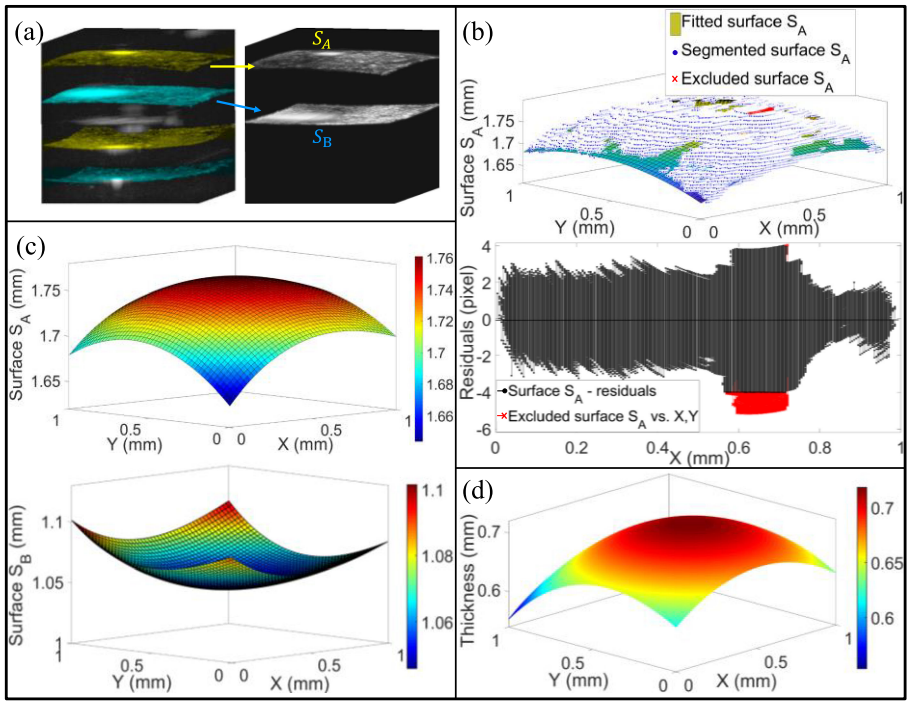

Fig. 6. (a) Left panel: 3D DSV-OCT image of IOL; Right panel: Distortion-free 3D image of IOL extracted from 3D DSV-OCT image. (b) Top panel: second order polynomial surface fitting of the experimental data of surface S_A; Bottom panel: residuals of the fitting; (c) Fitted surfaces S_A (top panel) and S_B (bottom panel) of 20D IOL sample; (e) Thickness map of 20D IOL sample.

TABLE 1
Measurement Obtained Using Different Degrees of IOLs

IOLs	Central Thickness (mm)	Refractive index	Dioptric Power (D)
5D	0.588±0.002	1.490±0.001	4.87±0.06
20D	0.712±0.002	1.491±0.0004	19.89±0.19
28D	0.992±0.002	1.491±0.001	27.82±0.45

in Fig. 6(c) and the thickness map is depicted in Fig. 6(d). The IOL's center thickness is determined to be 0.72 mm with the maxima in the thickness map. Finally, the IOL's dioptric power is determined according to Eq. (6), which is in compliance with the International Standard, ISO 11979-2:1999 Ophthalmic Implants-Intraocular Lenses, Part 2: Optical properties and test methods [28]. The measured values of the IOL is 19.89D, which is very close to the official value of 20D given in the manual.

Table 1 shows the measurement results of all the IOLs produced from five repeated measurements on each IOL, which is repositioned for each measurement. The averaged central thickness is 0.588 mm for 5D, 0.712 mm for 20D and 0.992 mm for 28D. The standard deviation (SD) is 0.002 mm for all the three IOLs, indicating a good consistent measurement accuracy. The refractive index (mean±SD) is 1.490±0.001 for 5D, 1.491±0.0004 for 20D, and 1.491±0.001 for 28D. Obviously, the refractive index measurement is quite consistent over the three IOLs and the SD is also very small. The measured refractive index is slightly smaller than the refractive index (1.492) provided by the manufacturer. This may be because our measurement is in near-infrared range while manufacturer determines the refractive index in visible range. The measured dioptric power (mean±SD) is 4.87±0.06D, 19.89±0.19D, and 27.82±0.45D for 5D, 20D and 28D IOLs,

respectively. Compared to the nominal values, the corresponding measurement errors are 0.13D, 0.11D, and 0.18D, respectively, which are well within the tolerances of the ISO Standard (0.3D for 0-15D, 0.4D for 15-25D, 0.5D for 25-30D) [28].

4. Discussion and Conclusion

In this work, to the best of our knowledge, we demonstrate the measurements of dioptric power, thickness and refractive index of IOL through a single volume OCT imaging for the first time. The proposed DSV-OCT overcomes the limitation with the existing method that IOL has to be flipped for imaging the two surfaces in sequence [25]. Usually, there are two common distortions in OCT imaging, one is lateral distortion due to the surface refraction, especially for curved surface, and the other is non-telecentric beam scanning (called field distortion in both lateral and axial dimension). For the former one, IOL's surface is imaged by exclusive surface reflection and consequently is not subject to any refraction-induced distortion. As for eliminating the field distortion, sample scanning is implemented to replace common beam scanning as reported in [25]. In addition, another advantage of our method is that it does not require rigorous sample alignment. For example, the effect of sample tilt on the measurement can be corrected in post processing as illustrated in Fig. 3. In comparison, confocal laser method requires IOL to be co-axised with measurement optic system [9].

Our method was evaluated on three IOLs with different dioptric powers. The measurement was repeated five times on each IOL. As discussed above, DSV-OCT can produce distortion-free three-dimensional topography of IOL as well as thickness distribution map. The standard deviation of center thickness measurement is 0.002 mm, which is comparable to the absolute accuracy of our DSV-OCT (0.003 mm) [26]. To measurement the refractive index, an A-scan is extracted from the three-dimensional image where the light hits IOL with normal incidence (the apex of the original 3D image of IOL). Consequently, the optical thickness extracted from this A-scan does not suffer any refraction and thus can be utilized with the physical thickness from DSV-OCT for calculating IOL's refractive index. In contrast, the refractive index measurement is likely to be affected by surface curvature for fiber-optic confocal microscope method [8]. As for dioptric power measurement, the measurement errors are well within the tolerances of the ISO Standard. This demonstrates the efficacy of our method. The measurement performance can be further improved by increasing the zero-padding size for the original spectrum to obtain more accurate surface identification in OCT image, which however has to pay the price of more computation time.

In conclusion, we demonstrated that DSV-OCT is well capable to measure the thickness, refractive index and dioptric power of IOLs with a good accuracy. Only one volume image is needed to achieve the measurements above. Moreover, the measurement is noncontact and computationally cheap, and also exhibits a good tolerance on measurement conditions, such as sample position and focus condition [26]. This makes our method is suited for IOL quality and production control. In addition, surface radius and shape can be obtained from DSV-OCT imaging without distortion, which is beneficial to further analyze and optimize the IOL design.

Acknowledgment

The authors wish to thank the anonymous reviewers for their valuable suggestions.

References

[1] WHO, "World report on vision," World Health Organization, Geneva, Switzerland, Aug. 2019. [Online]. Available: http://www.who.int/publications-detail/world-report-on-vision

[2] D. J. Apple, and J. Sims, "Harold ridley and the invention of the intraocular lens," *Surv. Ophthalmol.*, vol. 40, no. 4, pp. 279–292, Jan. 1996.

[3] R. F. Buenaga, and J. L. Alio, "Intraocular lens explantation after cataract surgery: Indications, results, and explantation techniques," *Asia Pac. J. Ophthalmol. (Phila)*, vol. 6, no. 4, pp. 372–380, 2017.

[4] J. C. Erie, M. H. Bandhauer, and J. W. McLaren, "Analysis of postoperative glare and intraocular lens design," *J. Cataract Refr. Surg.*, vol. 27, no. 4, pp. 614–621, 2001.
[5] N. E. Norrby *et al.*, "Accuracy in determining intraocular lens dioptric power assessed by interlaboratory tests," *J. Cataract Refr. Surg.*, vol. 22, no. 7, pp. 983–993, 1996.
[6] K. V. Sriram, M. P. Kothiyal, and R. S. Sirohi, "Direct determination of focal length by using talbot interferometry," *Appl. Opt.*, vol. 31, no. 28, pp. 5984–5987, 1992.
[7] E. Keren, K. M. Kreske, and O. Kafri, "Universal method for determining the focal length of optical systems by moire deflectometry," *Appl. Opt.*, vol. 27, no. 8, pp. 1383–1385, 1988.
[8] I. K. Ilev, "A simple confocal fibre-optic laser method for intraocular lens power measurement," *Eye*, vol. 21, no. 6, pp. 819–823, 2007.
[9] D.-H. Kim, D. Shi, and I. K. Ilev, "Alternative method for measuring effective focal length of lenses using the front and back surface reflections from a reference plate," *Appl. Opt.*, vol. 50, no. 26, pp. 5163–5168, 2011.
[10] F. G. Rauscher *et al.*, "Optical coherence tomography as a diagnostic tool for retinal pathologies in avian ophthalmology," *Invest. Ophth. Vis. Sci.*, vol. 54, no. 13, pp. 8259–8269, 2013.
[11] W. Drexler, and J. G. Fujimoto, "Optical coherence tomography in ophthalmology," *J. Biomed. Opt.*, vol. 12, no. 4, Jul. 2007, Art. no. 041201.
[12] J. Welzel, "Optical coherence tomography in dermatology: A review," *Skin Res. Technol.*, vol. 7, no. 1, pp. 1–9, 2001.
[13] B. E. Bouma, M. Villiger, K. Otsuka, and W. Y. Oh, "Intravascular optical coherence tomography," *Biomed. Opt. Express*, vol. 8, no. 5, pp. 2660–2686, 2017.
[14] T. H. Tsai, J. G. Fujimoto, and H. Mashimo, "Endoscopic optical coherence tomography for clinical gastroenterology," *Diagnostics (Basel)*, vol. 4, no. 2, pp. 57–93, 2014.
[15] M. J. Ju, S. J. Lee, E. J. Min, Y. Kim, H. Y. Kim, and B. H. Lee, "Evaluating and identifying pearls and their nuclei by using optical coherence tomography," *Opt. Exp.*, vol. 18, no. 13, pp. 13468–13477, 2010.
[16] R. Tong *et al.*, "Spectral-domain optical coherence tomography for the non-invasive investigation of the pigment layers of tang dynasty tomb murals exhibited in museums," *Optik*, vol. 199, 2019, Art. no. 163311.
[17] R. Su, M. Kirillin, E. W. Chang, E. Sergeeva, S. H. Yun, and L. Mattsson, "Perspectives of mid-infrared optical coherence tomography for inspection and micrometrology of industrial ceramics," *Opt. Exp.*, vol. 22, no. 13, pp. 15804–15819, 2014.
[18] S. Zhong *et al.*, "Non-destructive quantification of pharmaceutical tablet coatings using terahertz pulsed imaging and optical coherence tomography," *Opt. Lasers Eng.*, vol. 49, no. 3, pp. 361–365, 2011.
[19] X. Shao *et al.*, "Nondestructive measurement of conformal coating thickness on printed circuit board with ultra-high resolution optical coherence tomography," *IEEE Access*, vol. 7, pp. 18138–18145, 2019.
[20] N. Hirnschall, S. Amir-Asgari, S. Maedel, and O. Findl, "Predicting the postoperative intraocular lens position using continuous intraoperative optical coherence tomography measurements," *Invest. Ophth. Vis. Sci.*, vol. 54, no. 8, pp. 5196–5203, Aug. 2013.
[21] N. Hirnschall, T. Buehren, F. Bajramovic, M. Trost, T. Teuber, and O. Findl, "Prediction of postoperative intraocular lens tilt using swept-source optical coherence tomography," *J. Cataract Refr. Surg.*, vol. 43, no. 6, pp. 732–736, 2017.
[22] G. J. Tearney, M. E. Brezinski, J. F. Southern, B. E. Bouma, M. R. Hee, and J. G. Fujimoto, "Determination of the refractive index of highly scattering human tissue by optical coherence tomography," *Opt. Lett.*, vol. 20, no. 21, pp. 2258–2260, 1995.
[23] X. Wang, C. Zhang, L. Zhang, L. Xue, and J. Tian, "Simultaneous refractive index and thickness measurements of bio tissue by optical coherence tomography," *J. Biomed. Opt.*, vol. 7, no. 4, pp. 628–632, 2002.
[24] H. Y. Tang *et al.*, "Estimation of refractive index for biological tissue using micro-optical coherence tomography," *IEEE Trans. Biomed. Eng.*, vol. 66, no. 6, pp. 1803–1809, Jun. 2019.
[25] Y. Huang, K. Zhang, J. U. Kang, D. Calogero, R. H. James, and I. K. Ilev, "Noncontact common-path Fourier domain optical coherence tomography method for *in vitro* intraocular lens power measurement," *J. Biomed. Opt.*, vol. 16, no. 12, 2011, Art. no. 126005.
[26] Q. Wu, X. Wang, L. Liu, and J. Mo, "Dual-side view optical coherence tomography for thickness measurement on opaque materials," *Opt. Lett.*, vol. 45, no. 4, pp. 832–835, 2020.
[27] A. Podoleanu, I. Charalambous, L. Plesea, A. Dogariu, and R. Rosen, "Correction of distortions in optical coherence tomography imaging of the eye," *Phys. Med. Biol.*, vol. 49, no. 7, pp. 1277–1294, 2004.
[28] ISO, "Ophthalmic Implants-Intraocular Lenses-Part 2: Optical Properties and Test Methods," Int. Standards Org., Geneva, Switzlerand, ISO–119792, 1999.